CtFD Analysis of HTS Current Lead Fin-Type Heat Exchanger for Fusion Applications

Laura Savoldi Richard, Andreas Class, Walter H. Fietz, Reinhard Heller, Enrico Rizzo, and Roberto Zanino

***Abstract*—We apply a recently proposed Computational thermal Fluid Dynamics (CtFD) strategy to the analysis of a meander-flow path (MF) fin-type heat exchanger (HX), to be used in the HTS current leads for the LTS coils of both the W7-X stellarator and the JT-60SA tokamak. A mock-up of the HX was tested at the Karlsruhe Institute of Technology providing the database for the validation of the computational model. The hydraulic characterization of the mock-up is considered first, and then the heat transfer characteristic is analyzed.**

***Index Terms*—Computational fluid dynamics, current leads, heat exchangers, nuclear fusion.**

I. Introduction

THE stellarator Wendelstein 7-X (W7-X) is presently under construction in Germany and the tokamak JT-60SA is in the design phase within the framework of the ITER Broader Approach activities towards the DEMO reactor. Both machines will use HTS current leads for their magnet system [1], consisting of two main parts: an HTS module and a copper heat exchanger, covering the temperature range from 60 K to room temperature and actively cooled by He at 50 K. The heat exchanger is of the meander-flow (MF) path fin-type, consisting of a central copper bar with annular fins, as already used for the Large Hadron Collider at CERN [2], see Fig. 1.

Two different sub-size mock-ups of this HX were tested under different operating conditions at the Karlsruhe Institute of Technology [3] and a first computational thermal fluid dynamics (CtFD) analysis of the thermal characteristics of a sub-size mock-up was presented in [4]. The model assumed laminar flow conditions and a correlation for the Nusselt number as a function of Reynolds was developed.

Here we extend the work of [4], assessing the influence of turbulent versus laminar flow and validating the model against pressure-drop data, based on a periodic flow assumption which significantly reduces the computational cost. The turbulent model is then applied to the simulation of a thermal load in the full mock-up. The mock-up characterized by a distance of 3 mm between neighboring fins will be considered, while the fins are 2 mm thick.

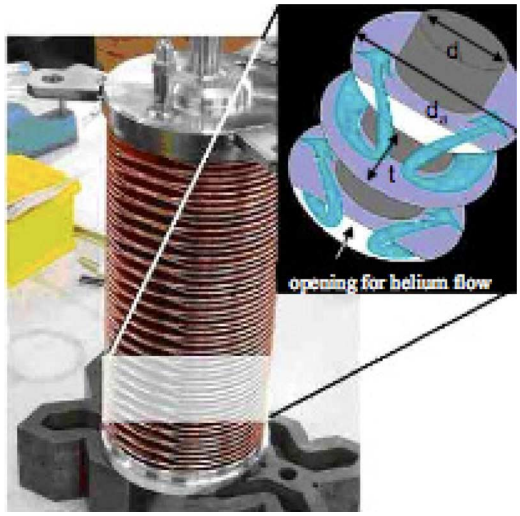

Fig. 1. Meander flow heat exchanger (He flow pattern in the inset).

II. Computational Model

The computational model describes the incompressible flow of the He in a 3-D domain, possibly coupled with heat conduction in the solid (fins, central Cu rod). Depending on the specific purpose of the analysis, either the full mock-up, including both the He and the copper solid structure, or a subset of this domain, including only the He between three neighboring fins (so-called double layer-DL), can be considered.

As the transition between laminar and turbulent regimes is not very clearly defined in such a complex geometry, we wish to investigate the effect of different assumptions on the flow regime. In the turbulent case we choose a low-Re linear $k-\varepsilon$ model with so-called hybrid wall treatment [5], which has the advantage of not requiring special grid refinement at the wall. For the sake of simplicity, the 3-D domain was meshed by first meshing the generic 2-D domain on a plane perpendicular to the HX axis (three increasing planar resolutions, defined below as $1\times$, $2\times$ and $4\times$ were used, with 7832, 30684 and 121460 nodes, respectively, when the solid is also included); then this grid is repeated at uniform axial steps. Axial grids with the distance between two successive planes equal to 1, 1/2, 1/4 mm, for the full mock-up case including the solid, and further on to 1/8, 1/16 and 1/32 mm, for the periodic case not including the solid, were used. The above implies that a typical (1/4 mm, $1\times$) 3-D grid of the full mock-up has $\sim$2 Mcells, while the finest (1/16 mm,

Manuscript received October 21, 2009. First published March 25, 2010; current version published May 28, 2010.

E. Rizzo, L. Savoldi Richard, and R. Zanino are with Dipartimento di Energetica, Politecnico di Torino, 10129 Torino, Italy (e-mail: laura.savoldi@polito.it).

A. Class is with Institut fuer Kern- und Energietechnik, Karlsruhe Institute of Technology, 76021 Karlsruhe, Germany.

W. H. Fietz and R. Heller are with Institut fuer Technische Physik, Karlsruhe Institute of Technology, 76021 Karlsruhe, Germany.

Color versions of one or more of the figures in this paper are available online at http://ieeexplore.ieee.org.

Digital Object Identifier 10.1109/TASC.2010.2041546

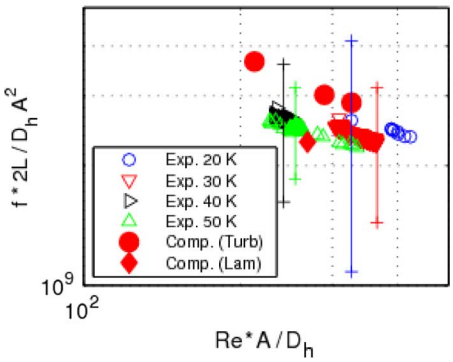

Fig. 2. Dimensional friction factor versus dimensional Reynolds number.

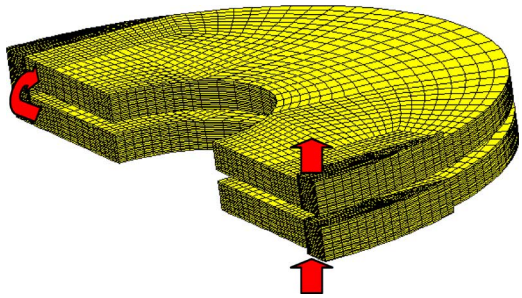

Fig. 3. Computational domain (double layer) for the periodic flow model showing the (1/4 mm, 1×) grid on the surface of the domain. The refined regions on the foreground refer to the inlet and outlet sections; the arrows identify the main flow direction.

4×) 3-D grid used here for the periodic flow model of a DL has ∼2.5 Mcells.

The device is assumed to operate in steady state conditions.

The model is implemented and solved within the commercial software Star-CD [6].

III. Validation Against Pressure Drop Data

A. Experimental setup

The pressure drop Δp was measured for a few different mass flow rates (dm/dt) at different inlet temperatures between 20 K and 50 K. During these tests the pressure was not kept constant but varied in time, in some cases quite significantly. However, since this variation is not too large with respect to Δp and considering it occurs over time scales sufficiently longer that the transit time of the He in the mock-up (estimated to be ∼4 s), we can assume quasi-steady state operating conditions.

Δp and (dm/dt) are related to the friction factor f and the Reynolds number Re by the usual relations:

$$Re = (dm/dt)D_h/(\mu A) \quad (1)$$

$$f = (1/2)(\Delta p/L)\rho D_h A^2/(dm/dt)^2 \quad (2)$$

where μ is the dynamic viscosity and ρ is the density of the fluid. Therefore, even without committing on a specific definition of cross section A, hydraulic diameter D_h, and hydraulic length L, which choice could be delicate in view of the complex geometry of this HX, the data can still be collected in pseudo-dimensionless form as shown in Fig. 2, where we see that the points at different p and T cluster around a single line, if the experimental error on pressure difference (∼500 Pa) is taken in account.

B. Periodic Model Assumptions

In these tests we can assume the flow to be periodic, such that the flow speed distribution at an inlet section (cutting the midplane of a fin) coincides with that at the outlet section two fins downstream, see Fig. 3; the same is true for the pressure distribution, but for a constant Δp (this set of boundary conditions is called partially cyclic in the Star-CD jargon); we call this portion of the HX a double layer (DL). Also symmetry around a plane passing through the HX axis and cutting into two equal parts the meander is considered. An additional (anti-) symmetry is present, which would allow us to further reduce the size of the domain (and correspondingly the needed number of grid points), by another factor of two, reducing it to (half of) the volume between *two* neighboring fins. However this was not done so far, because it requires a revision of the mesh generation procedure. Finally, the solid can be excluded from the problem in this case, with a substantial reduction in problem size: on the cell faces that would belong to the fluid-solid interface, we now impose so-called "wall" boundary conditions [5].

In the "computational experiment" we typically impose (dm/dt) and compute Δp, but also the opposite procedure is possible and, indeed, it sometimes converges faster (to the same solution).

C. Results

The results of our analysis for the case of a turbulent flow model are also shown in Fig. 2. For these points, numerical convergence was verified, see the Appendix. It is seen that there is a good agreement between simulation and measurement, with a little overestimation of the experimental Δp, which may be considered within the experimental error bar. For the sake of completeness and reference we also show the Δp computed with a laminar flow model: although the two models give results that are both within the experimental error bar, in principle the use of a turbulent model appears mandatory in this case, because the computed ratio between turbulent and dynamic viscosity is up to ∼100 (not shown).

Figs. 4–6 show the computed flow field between two neighboring fins. Large recirculation regions develop at the downstream corners, while the flow detaches and accelerates as it turns around the leading edge of the fin. This feature will obviously give a significant contribution to the pressure drop.

On the contrary, in horizontal planes the flow field does not show a significant detachment from the surface of the central Cu bar, with only minor recirculation downstream, see Fig. 6; therefore it is to be expected that the central Cu bar will not give a significant contribution to the total pressure drop.

IV. Thermal Analysis

A. Validation Against Thermal Data (Full Mock-Up)

The experimental setup and data presented in [4] have been considered here for the purpose of validating the CtFD model of the full mock-up. Unfortunately in this case only a limited resolution of the grid is affordable, as the full mock-up is made of 24 DLs and also the solid must be included in the model.

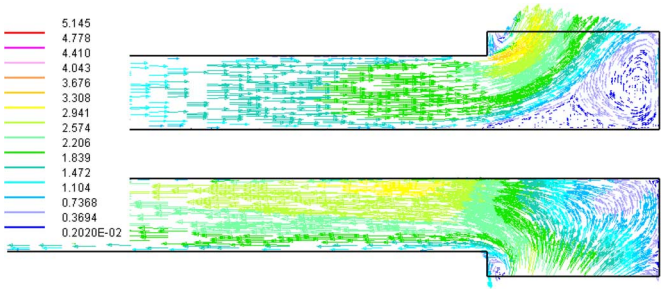

Fig. 4. Computed flow field between two neighboring fins: vertical cut including inlet and outlet regions. Flow is from the bottom to the top. (1/16 mm, 4×) grid.

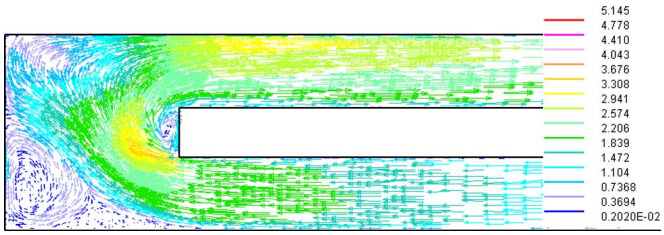

Fig. 5. Computed flow field between two neighboring fins: vertical cut including corner region with transition from the lower part to the upper part of the fin. Flow is from bottom to top. (1/16 mm, 4×) grid.

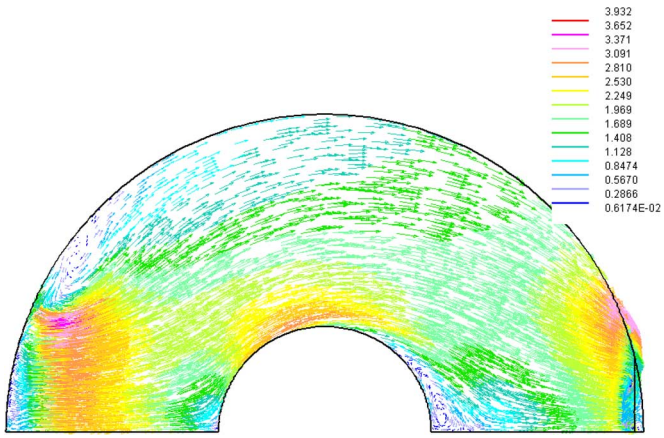

Fig. 6. Computed flow field between two neighboring fins: horizontal (midplane) cut including central copper rod. Flow is from left to right. (1/16 mm, 4×) grid.

A constant heat source is applied inside the Cu bar at the He outlet side of the HX; the Cu temperature at the inlet and outlet side is used as boundary condition, together with the He inlet temperature; a good agreement between the measured He outlet temperature and the result of the computation, shown in Fig. 7, validates the model. The disagreement at the He outlet decreases with the (axial) grid size as expected (not shown).

B. Verification of Local (Periodic) CtFD Model

The similar approach as outlined in Section III-B for the simulation of the hydraulic characteristic can be extended to the CtFD simulation. In this case we assume given temperature $\mathrm{T_{wall}}$ at all walls, except on the outer (cylindrical) surface where

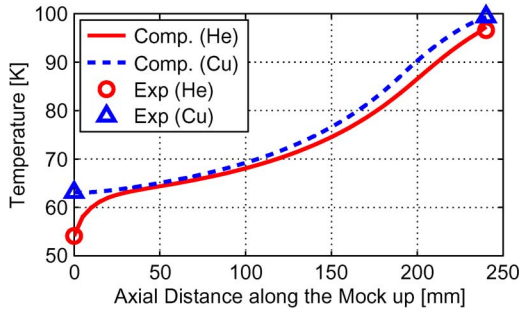

Fig. 7. Comparison between computed temperature profiles in the full mock-up and measured boundary values, (1/8 mm, 1×) grid.

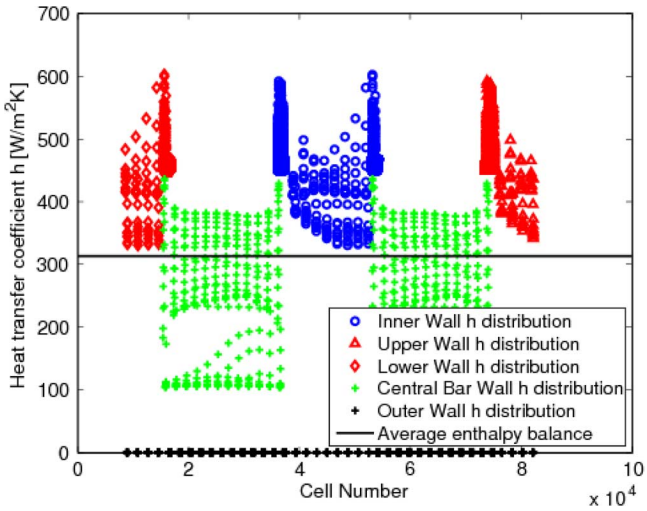

Fig. 8. Computed distribution of the local heat transfer coefficient H on different wall surfaces for $\mathrm{T_{wall}} = 75\ \mathrm{K}$, $(\mathrm{dm/dt}) = 1.36\ \mathrm{g/s}$, (1/4 mm, 1×) grid. The value $\langle \mathrm{H} \rangle$ estimated from the enthalpy balance over the whole DL is also shown for comparison.

an adiabatic condition is enforced; by adopting this strategy, the periodic domain does not include the solid.

For given mass flow rate and inlet temperature, the thermal characteristic of a DL can be derived, using $\mathrm{T_{wall}}$ as parameter, from which a Nu (Re) will be deduced, applicable on average to the whole DL. Nu is defined here based on the average heat transfer coefficient $\langle \mathrm{H} \rangle$, which is computed using an overall enthalpy balance. This $\langle \mathrm{H} \rangle$ can also be compared with the direct result of the CtFD calculation, which provides the *local* H for each wall cell, see Fig. 8. Fig. 8 verifies the above-mentioned antisymmetry of the problem and also highlights that the heat transfer is more efficient on the (horizontal) fin surfaces than on the (vertical) surface of the central Cu bar; it additionally shows that on the fins the most effective areas for heat transfer (local peaks in Fig. 8) are those just downstream of the turn, where indeed the peak turbulent kinetic energy arises (not shown).

The (dimensional, see above) Nu (Re) obtained by repeated application of the periodic model for different $\mathrm{T_{wall}}$ values compares within 10% or so, see Fig. 9, with the Nu (Re) that can be derived from the enthalpy balances on the single DLs based on the results of Section IV-A. This agreement will eventually justify the use of the local CtFD approach for deriving a correlation

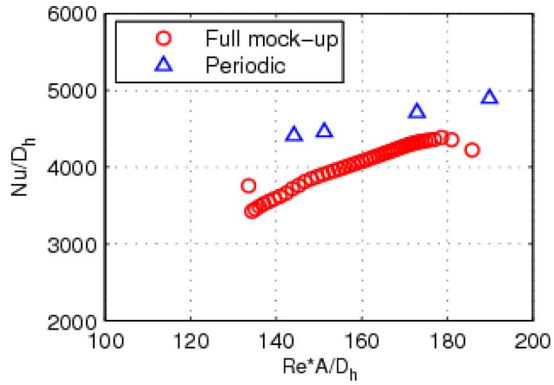

Fig. 9. Comparison between Nu (Re) correlation deduced from the full mock-up simulation of Section IV-A and the local analysis based on the periodic CtFD model.

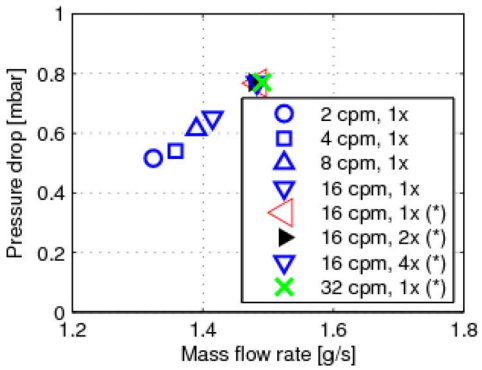

Fig. 10. Grid independence of the turbulent model solution. Either the mass flow rate, or the pressure drop (cases denoted with $(*)$ in the legend) was imposed.

applicable to the case when also the heat source due to current flowing in the central Cu bar is present.

V. Conclusions and Perspective

The hydraulic and thermal performance of a HX mock-up for HTS current leads aimed at different fusion applications was analyzed using the commercial code Star-CD.

Good agreement between CFD computation and pressure drop measurement was shown, as well as between CtFD computation and thermal measurement.

In perspective, the periodic model approach shall be applied to the derivation of a correlation for full-size HX optimization.

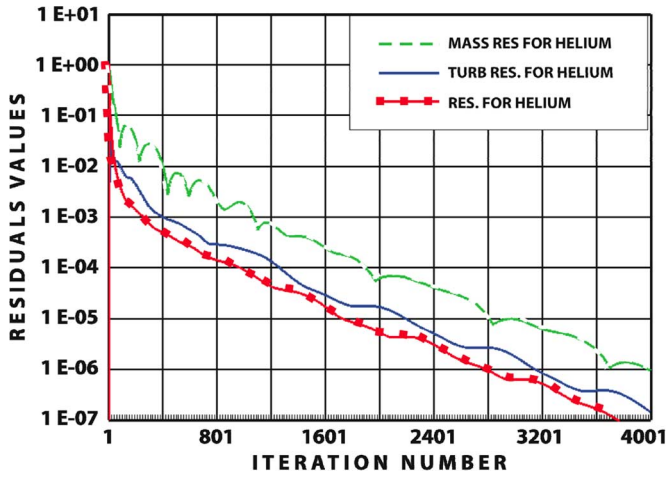

Fig. 11. Convergence of the residuals on the (1/16, 4×) grid.

Appendix

The numerical convergence of the pressure drop results presented above in Fig. 2 is demonstrated by the increasing independence of the solution for a given value of $\mathrm{Re} * \mathrm{A}/\mathrm{D_h}$ as the grid is refined, see Fig. 10, and by the behavior of the residuals of the different (mass, momentum, turbulent) equations on, e.g., the finest relevant grid (1/16 mm, 4×), see Fig. 11.

Acknowledgment

ER thanks the Karlsruhe Institute of Technology for kind hospitality during his Master's Thesis preparation, which contributed to the present work. We thank CDAdapco Italy for providing the Star-CD licenses at Politecnico di Torino.

References

[1] W. H. Fietz, R. Heller, A. Kienzler, and R. Lietzow, "High temperature superconductor current leads for WENDELSTEIN 7-X and JT-60SA," *IEEE Trans. Appl. Superconductivity*, vol. 19, no. 3, pp. 2202–2205, Jun. 2009.

[2] A. Ballarino, S. Mathot, and D. Milani, "13000-A HTS current leads for the LHC accelerator: From conceptual design to prototype validation," in *Proc. of Eucas 2003*, Sorrento, Italy, LHC Project Report 696.

[3] R. Lietzow, R. Heller, and H. Neumann, "Performance of heat exchanger models in upside-down orientation fort he use in HTS current leads for W7-X," in *Advances in Cryogenic Engineering: Trans. of the Cryogenic Engineering Conference—CEC*, 2008, vol. 53, pp. 1243–1250.

[4] R. Heller, A. Class, A. Batta, R. Lietzow, H. Neumann, and M. Tischmacher, "Modelling of the fin type heat exchanger for the HTS current leads of W7-X and JT-60SA," *Cryogenics*, accepted for publication.

[5] CD-adapco, Methodology ver. STAR-CD version 4.06, 2008.

[6] CD-adapco, ver. STAR-CD version 4.06, 2008.